EPJ manuscript No.
(will be inserted by the editor)

Energy-dependent diffusion in a soft periodic Lorentz gas

S. Gil-Gallegos[1,a], R. Klages[1,2,3,b], J. Solanpää[4,c], and E. Räsänen[4,d]

[1] Queen Mary University of London, School of Mathematical Sciences, Mile End Road, London E1 4NS, UK
[2] Institut für Theoretische Physik, Technische Universität Berlin, Hardenbergstraße 36, 10623 Berlin, Germany
[3] Institute for Theoretical Physics, University of Cologne, Zülpicher Straße 77, 50937 Cologne, Germany
[4] Laboratory of Physics, Tampere University of Technology, Tampere FI-33101, Finland

Abstract. The periodic Lorentz gas is a paradigmatic model to examine how macroscopic transport emerges from microscopic chaos. It consists of a triangular lattice of circular hard scatterers with a moving point particle. Recently this system became relevant as a model for electronic transport in low-dimensional nanosystems such as molecular graphene. However, to more realistically mimic such dynamics, the hard Lorentz gas scatterers should be replaced by soft potentials. Here we study diffusion in a soft Lorentz gas with Fermi potentials under variation of the total energy of the moving particle. Our goal is to understand the diffusion coefficient as a function of the energy. In our numerical simulations we identify three different dynamical regimes: (i) the onset of diffusion at small energies; (ii) a transition where for the first time a particle reaches the top of the potential, characterized by the diffusion coefficient abruptly dropping to zero; and (iii) diffusion at high energies, where the diffusion coefficient increases according to a power law in the energy. All these different regimes are understood analytically in terms of simple random walk approximations.

1 Introduction

The need for smaller and more efficient electronic devices challenges both science and technology by pushing their boundaries. In order to understand the structure and dynamics of matter on very small scales, simple mathematical models have been constructed. An important example concerns the transport of matter by diffusion: Typically this problem is studied by methods of conventional non-equilibrium statistical mechanics, where a stochastic process is assumed to govern the collisions between particles. However, starting from microscopic deterministic equations of motion helps to understand the origin of diffusion within the framework of dynamical systems theory. Employing this approach it is possible to derive a macroscopic irreversible process out of reversible microscopic equations of motion [1–3].

By understanding diffusion in simple dynamical systems it is possible to learn about the transport properties of more complex models. For example, in piecewise linear one-dimensional chaotic maps it has been found that the diffusion coefficient is a fractal function of control

[a] e-mail: s.gilgallegos@qmul.ac.uk
[b] e-mail: r.klages@qmul.ac.uk
[c] e-mail: janne@solanpaa.fi
[d] e-mail: esa.rasanen@tut.fi

parameters [4–6]. A relatively simple two-dimensional map with similarly irregular diffusion coefficients is the standard map [7,8], which can be derived as a time discrete version of a chaotic nonlinear pendulum equation [9,10]. Here it has been observed that normal diffusion is interrupted by regions in parameter space which are related to accelerator modes yielding superdiffusive transport [11–13]. Normal diffusion means that the mean square displacement of an ensemble of particles increases linearly with time while superdiffusion refers to a time dependence that grows faster than linear in time. A nonlinear time dependence of the mean square displacement is generally called anomalous diffusion [14].

Another class of dynamical systems with highly interesting transport properties is given by Hamiltonian particle billiards [15]. In the paradigmatic two-dimensional Lorentz gas a point particle performs specular reflections with circular scatterers distributed in the plane [16]. Originally constructed to model the motion of electrons in metals, the Lorentz gas has been widely investigated from both mathematical and physical points of view [1–3,17,18]. In periodic versions of the Lorenz gas it has been found that the diffusion coefficient is an irregular function of the density of scatteres as a parameter [19–21]. This relates to the line of work on irregular parameter-dependent diffusion coefficients in simple maps referred to above. However, it is an open question whether the diffusion coefficient in the periodic Lorentz gas exhibits a fractal structure under variation of control parameters [3,22]. A related billiard is a one-dimensional corrugated floor, where a particle experiences a vertical force and collides with arcs positioned horizontally [23]. Here the diffusion coefficient was numerically computed as a function of the energy, and islands in phase space were found for particular energies yielding superdiffusion. When no islands were present diffusion was normal. Altogether the diffusion coefficient displayed an intricate dependence on the energy. A related systems was the bouncing ball billiard, where a particle diffused on a vibrating corrugated floor by losing energy at collisions. Again diffusion was detected numerically to be highly irregular under variation of the particle's energy [24]. All these studies point to the conjecture that under certain conditions the diffusion coefficient in deterministic dynamical systems may exhibit a non-trivial, often fractal-like dependence on control parameters [5,3,25].

To model more realistic particle collisions, the hard Lorentz gas scatterers should be softened. When the walls of a scattering billiard are smoothened by using a soft repulsive potential, periodic orbits appear near a special class of trajectories in the original system [26,27]. These new periodic orbits are accompanied by periodic islands of stability yielding a mixed phase space. As a mixed phase space is decomposable into disjoint invariant sets, ergodicity is no longer present in such systems [28]. Singular trajectories inducing islands of stability in the phase space have also been reported for atom-optic billiards studied both numerically and experimentally [29]. For periodic billiards with scatterers softened by attractive Coulombic potentials, a mathematical proof states that for energies above a certain threshold the motion of particles is diffusive [30]. By exploring the dependence of the diffusion coefficient D on the energy E in such a system a relation of $D(E) \sim E^{3/2}$ for large energies has been derived [31]. Moreover, a soft inelastic periodic Lorentz gas with time-dependent scatterers was proposed in Ref. [32]. Here it was found that the diffusion coefficient grows like $D(E) \sim E^{5/2}$ for large energies. In both cases results from computer simulations were supported by constructing different simple random walk models from which the diffusion coefficient could be calculated analytically as a function of the energy.

Different models were considered to replace the hard walls in Lorentz gases by soft potentials, most notably by using trigonometric functions yielding an egg-crate potential [33–37], by a Lennard-Jones potential [38], or simply by a finite potential height [39]. The first type of systems was designed to model experiments on electrons in lateral superlattices under magnetic fields [35]. Here it was experimentally observed that the magnetoresistance varies highly irregularly as a function of the magnetic field strength [40,41]. It was then shown in computer simulations combined with dynamical systems and stochastic theory that specific peaks in the magnetoresistance are due to periodic orbits with associated islands of stability in phase space, which correspond to electrons circling around specific sets of scatterers [42,43]. A similar type of system that attracted much attention recently is artificial graphene, where electrons are confined to a hexagonal configuration of scatterers by using, e.g., semiconductor quantum dots [44,

45] or molecules on a metallic surface [46,47]. The latter system is often referred to as molecular graphene, which is topologically equivalent to the triangular Lorentz gas. Hence, the study of periodic billiard systems with soft potentials has direct relevance not only in the theory of dynamical systems and diffusion, but also in present nanotechnology.

In this work we study the diffusion coefficient as a function of the energy as a control parameter in a soft Lorentz gas. While in a conventional hard-wall system the energy generates only a trivial scaling of the diffusion coefficient, as the velocity is constant, the scenario is completely different for a soft potential. In a recent work by the present authors [48] it was shown that a soft Lorentz gas modeled by Fermi potentials exhibits an intricate interplay between normal and anomalous diffusion as a function of the density of scatterers. Here we investigate the same system, however, we are now interested in its diffusive properties under variation of the energy of the moving particle as a control parameter while we keep the density of scatterers fixed. We resort to extensive numerical simulations supplemented by analytical random walk approximations to explain our numerical results.

Our article is organized as follows: In Sec. 2 we construct a softened version of the Lorentz gas and describe our numerical methods. In Sec. 3 we present our simulation results in the small-energy regime, where we develop *ad hoc* random walk approximations for the diffusion coefficient based on a simple phase space argument [49] as well as on a collision length approach. In Sec.4 we explore an intermediate regime where the energy is close to the maximum of a scatterers and derive another random walk model. In Sec. 5 we characterize the asymptotic form of the diffusion coefficient for high energies. We also discuss the complicated structure of the phase space and the appearance of islands of stability by varying the energy parameter. Finally, in Sec. 6 we conclude our work and present open questions.

2 Model and numerical methods

2.1 Soft Lorentz gas

For our study we use the soft model introduced in Ref. [48], which has the advantage that it reproduces the conventional triangular Lorentz gas with hard circular scatterers in a specific limit of the softness parameter. For this model each circular scatterer is defined by a Fermi potential of the form

$$V_{\mathrm{F}}(r) = \frac{1}{1+\exp\left(\frac{|\mathbf{r}|-r_o}{\sigma}\right)}, \tag{1}$$

where σ and r_o are the softness and the radius of a scatterer, respectively. The complete potential field consisting of an infinite triangular array of scatterers is given by

$$V(\mathbf{r}) = \sum_n V_{\mathrm{F}}(\mathbf{r}-\mathbf{r}_n), \tag{2}$$

where $\mathbf{r}_n$ is the position vector to the n-th point of the lattice in the plane. The maxima and minima of the potential are located at the vertices and centers of the triangles, respectively, whereas the edges of the triangles have saddle points; see Fig. 1.

If the particle has total energy $E > E_*$ it can escape from the region enclosed by three scatterers through the available space between $r(E)$ and $r(E) + W(E)$, where the gap $W(E)$ is given by

$$W(E) = L - 2r(E). \tag{3}$$

Here L is the fixed distance between the centres of two adjacent scatterers. This scenario is visualized in Fig. 1.

The exact radius r should be computed by considering the contribution of all potentials located at each point of the lattice. If we use the contribution of two adjacent potentials as shown in Fig. 1, it would be necessary to solve for $r(x)$ and $r(x-L)$ when $V_1(x) + V_2(x) = E$. Alternatively, considering only $V_1(x)$ we can obtain an analytical expression for the radius. By

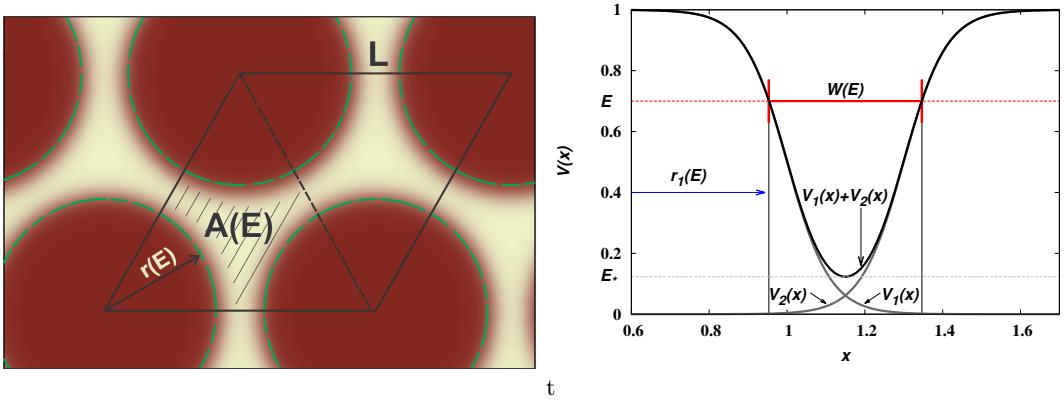

Fig. 1. Left panel: Profile of the potential of our soft Lorentz gas defined in Eqs. (1) and (2). $A(E)$ is the area inside a unit cell enclosed by equipotential lines with radius $r(E)$, where E is the total energy of a particle. Right panel: Potential $V = V_1 + V_2$ along the x-axis (bottom boundary of the parallellogram unit cell in the left panel). The gap size $W(E)$ and the radius $r_1(E)$ are defined by the energy E, cf. Eqs. (3) and (4). E_* holds for the energy threshold as explained in the text.

solving $V_1(x) = E$ for $r(x)$ we get the radius in terms of the energy. For simplicity we will label this new radius with r_1, and it is given by

$$r_1(E) = \sigma \ln(1/E - 1) + r_o. \tag{4}$$

Note that due to the overlapping potentials the radius r_1 is an underestimation of the real radius r in Eq. (3), since r_1 has been computed considering only one potential. Hence, the real gap size $W(E)$ given by Eq. (3) with r_1 yields an overestimation. This effect is enhanced when $E \to E_*$, as the difference $r - r_1$ increases.

Finally, we connect $W(E)$ with the separation of the scatterers in the hard Lorentz gas w. These two quantities are related by the lattice length

$$L = 2r_o + w = 2r(E) + W(E),$$

where r_0 is the radius of a hard Lorentz gas scatterer and w is the minimal distance, or gap size, between two adjacent scatterers. Therefore we can use either the parameter L or w to define the density of the scatterers. In our random walk model introduced in Sec. 3 we use the radius of Eq. (4), bearing in mind that there is a greater error the closer E is to the threshold E_*. In this work we set the softness parameter in Eq. (1) to $\sigma = 0.01$ and the lattice distance to $L = 2r_o + w$ with $r_o = 1$ and $w = 0.05$. These values enable normal diffusion in a relatively large interval of energies as discussed in detail in Sec. 5.

2.2 Computation of the diffusion coefficient

The diffusion coefficient is defined by [1–3]

$$D = \lim_{t\to\infty} \frac{\langle(\mathbf{r}(t) - \mathbf{r}(0))^2\rangle}{4t}, \tag{5}$$

where $\mathbf{r}(t)$ is the position of a particle at time t and $\langle(\mathbf{r}(t) - \mathbf{r}(0))^2\rangle$ yields the mean square displacement (MSD) with the ensemble average of particles denoted by the angular brackets. If the limit in Eq. (5) exists or, equivalently, the growth of the MSD is linear in time, we have normal diffusion.

According to Eq. (5) one can obtain D from calculating the MSD. For our model we first computed the MSD from computer simulations, which were carried out with the bill2d software

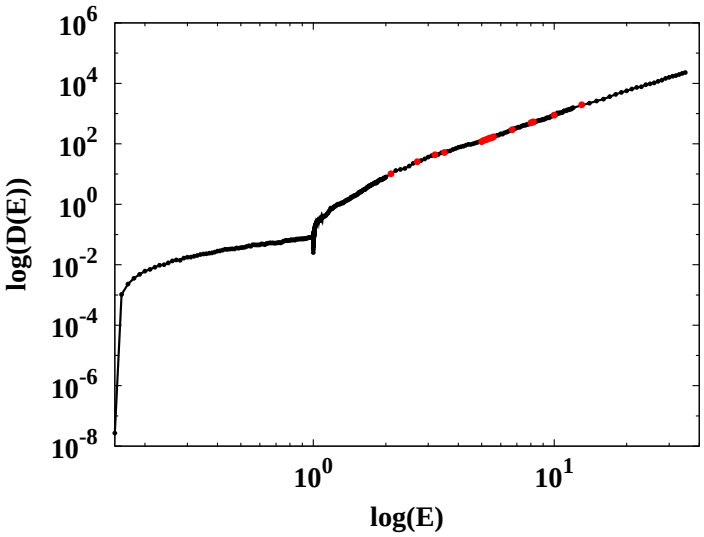

Fig. 2. Diffusion coefficient D as a function of energy E in a double-logarithmic plot obtained from simulations according to Eq. (5); see the text for the simulation parameters. Red circles denote energies where the model exhibits superdiffusion, i.e., $D(E)$ does not exist.

package [50] at different values of the energy. The force acting on the particles is given by the gradient of Eq. (2). Here we sum only over lattice points of scatterers that are in a rhomboid unit cell, see Fig. 1. An ensemble of particles is uniformly distributed in the coordinate space associated to such a unit cell. Trivially, only energetically valid combinations of (x, y, v_x, v_y) are allowed. In an ergodic dynamical system the selection of initial conditions is not important, as in the long run all regions in phase space will be sampled for any given initial condition [1]. However, since in Hamiltonian dynamical systems with a mixed phase space ergodicity is broken, cf. our discussion in Sec. 1, we need to make sure that our ensemble of initial points is large enough such that it adequately samples different disjoint regions in phase space to reflect the full dynamics [28].

For reliably extracting the MSD from simulations we use the following input parameters: For energies $E < 2$ the computing time is $t = 5000$ and the ensemble size of the particles $N = 20000$. For energies $E > 2$ we set the ensemble size to $N = 40000$ and the iteration time to $t = 40000$. The time step is $\Delta t 10^{-3}$. By increasing the ensemble size, using a smaller time step, etc., we have tested that these parameter values yield good convergence of the MSD to an asymptotic limit where it grows linearly in time t in parameter regions (w, σ) where islands in phase space do not seem to exist [52]. In Fig. 2 we present results for the diffusion coefficient obtained from simulations. We can distinguish two different regimes for small and large energies, as well as a distinctive transition point around $E = V_{\max} = 1$. In the following we will analyse these different regimes in full detail. We also note that there are parameter values where the diffusion coefficient was not computable from simulations, that is, the MSD did not reach a linear regime within the computing time. These parameter regions where the MSD grows faster than linear are marked as red dots. We elaborate on the physical mechanism generating this specific dynamics in Sec. 5 below.

3 Diffusion coefficient for small energies

In previous literature random walks have been used as simple models to reproduce analytically computer simulations results for the diffusion coefficient in the hard Lorentz gas as a function of the density of scatterers [49,19,21]. This comparison clarifies whether the deterministic diffusive dynamics generated in the chaotic Lorentz gas can be understood in terms of a simple

stochastic process, which elucidates the origin and the type of the diffusive dynamics. On this basis similarities and differences between deterministic and stochastic diffusive processes can be explored [1–3]. In this section we test to which extent the diffusion coefficient in our soft Lorentz gas can be explained by simple random walks for small energies, i.e., close to the onset of diffusion. For this purpose we construct a random walk model for diffusion as a function of the energy and compare our analytical results to computer simulations.

3.1 Analytical random walk approximations

For small energies $E < V_{\max} = 1$ we first approximate the diffusion coefficient as a function of the total energy by means of a phase space argument [49,19,21], and secondly employing a collisionless flight or Boltzmann approach [19]; see also Ref. [48]. For random walks on two-dimensional lattices the diffusion coefficient is obtained from

$$D = \frac{l^2}{4\tau}, \tag{6}$$

where l is the distance travelled in one step during the time interval τ of the random walk.

In order to construct a random walk model by using this equation, the starting point is to identify what we call a "trap" in our model. In the soft Lorentz gas this is the region that is available for a particle in the position space inside a triangular unit cell, orresponding to what was called a trap in the hard Lorentz gas [49,19,21]. As is shown in the left panel of Fig. 1 there are three exits from a trap. The width of an exit, respectively the minimal gap size between two nearby scatterers, is defined in the right panel of Fig. 1.

3.1.1 Machta-Zwanzig random walk and phase space argument

According to a random walk approximation put forward by Machta and Zwanzig [49], a particle travels from one trap to another by a random walk yielding the diffusion coefficient of Eq. (6). For a soft Lorentz gas the escape time τ expressed in terms of the energy E leads to

$$D_{\mathrm{MZ}}(E) = \frac{l^2}{4\tau(E)}, \tag{7}$$

where the distance l between two adjacent traps is constant, as we are not including a variation of the lattice. Hence, l can be calculated by geometrical means. The average escape time from a trap τ^{-1} is given by the quotient of the total phase space Ω and the fraction of phase space ω that escapes from the gap during time τ,

$$\tau^{-1} = \frac{\omega}{\Omega}. \tag{8}$$

Here the velocity space is $2\pi v(E)$, where $v(E)$ is to be determined. The total volume of the phase space is thus

$$\Omega = A_{\mathrm{trap}} 2\pi v(E), \tag{9}$$

where A_{trap} is the area available in position space which is also a function of the energy, $A_{\mathrm{trap}} = A(W(E))$. This area depicted in Fig. 1 depends on the radius $r_1(E)$ as expressed by Eq. (4).

We can calculate the available area for a particle in the position space by geometrical means in analogy to the conventional (hard-wall) Lorentz gas. The area is determined by the equipotential lines with $V_1(r) = E$ and the three exits of the trap. We take the area of the unit cell and subtract three times the area formed by semicircles with radius $r_1(E)$ as in Eq. (4). We find that $A(W(E))$, simplified to $A(E)$, is given by the expression

$$A(E) = \sqrt{3}(2r_o + w/2)^2 - \frac{\pi}{2}(\sigma \ln(1/E - 1) + r_o)^2.$$

Strictly speaking $A(E)$ has a more complicated dependence on E due to the overlapping of the potentials. However, here we use $A(E)$ as a first approximation. where is the angle between the velocity vector at the moment of exiting the unit cell and the normal to the boundary dening the gap; the speed jvj = v needs to be determined. Let us suppose that the velocity v of a particle is constant at the moment of exiting a trap. Then the particle flux is given by

$$\int |\mathbf{n}||\mathbf{v}| \cos\theta v d\theta = 2v^2, \tag{10}$$

where θ is the angle between the velocity vector at the moment of exiting the unit cell and the normal to the boundary defining the gap; the speed $|\mathbf{v}| = v$ needs to be determined. There are three exits of width $W(E)$ leading to

$$\omega = 3W(E)2v^2(E). \tag{11}$$

Substituting these quantities into Eq. (8) and proceeding with Eq. (7) yields our final result

$$D_{\mathrm{MZ}}(E) = \frac{3l^2 W(E)}{4\pi A(W(E))} v(E). \tag{12}$$

3.1.2 Random walk approximation based on collisionless flights

We now construct a second random walk approximation, which is based on collisionless flights. The starting point is the formula

$$D_{\mathrm{B}} = \frac{l_c^2}{4\tau_c} \tag{13}$$

for the diffusion coefficient, where τ_c stands for the mean free time between collisions and l_c is the corresponding mean free path between collisions. Note that in systems composed of smooth potentials strictly speaking collisions are not defined, as at any instant of time there is a force acting on the particle. For the following approximate analytical calculations, we thus define a collision for a particle with total energy E as the moment where it hits an equipotential line of energy E. We remark, however, that for computational purposes (not carried out here) one should define a collision differently, e.g., by a particle having a zero velocity component perpendicular to an equipotential line. In order to calculate τ_c for the soft Lorentz gas we straightforwardly adapt the phase space argument of Eq. (8): Instead of considering the length of the exits to calculate ω we replace them by the length of the walls inside the trap. For this we use the arc length that originates from the angle $\pi/3$ and the radius $r(E)$ of the equipotential line determined by $V(r) = E$. There are three arcs leading to $l = \pi r(E)$ and

$$\omega = \pi r(E) 2v^2(E),$$

in analogy to Eq. (11). The total volume of the phase space Ω is the same as in Eq. (9). If an average constant velocity v is assumed as before, then

$$\tau_c = \frac{A(W(E))}{r(E)v}. \tag{14}$$

Considering an average velocity given by $v_{\mathrm{ave}} = l_c/\tau_c$, substituting $l_c = \tau_c v_{\mathrm{ave}}$ in Eq. (13) and using Eq. (14) leads to our final expression

$$D_{\mathrm{B}}(E) = \frac{A(W(E))}{4r(E)} v_{\mathrm{ave}}(E). \tag{15}$$

3.2 Estimation of the velocities at the exit of a trap

Generally the velocity of a particle in a soft Lorentz is not constant, and it is not possible to obtain analytical forms for it. Here we work out three approximations for the velocity when a particle leaves a trap.

1. We assume that a particle has a maximum velocity at the moment of exiting a trap. Using energy conservation we find
$$v(E) = \sqrt{2(E - V(r))}.$$
The potential is given by Eq. (1) at each point of the lattice. Consider the base of a triangle in the array as the x-axis and let us take into account the contributions of two adjacent potentials V_1 and V_2, as shown to the right of Fig. 1. For simplicity we continue our analysis by considering only the contribution of the potential on the x-axis, denoted as
$$V(x) = V_1(x) + V_2(x) = \frac{1}{1 + \exp((|x| - r_o)/\sigma)} + \frac{1}{1 + \exp(|x - L| - r_o)/\sigma)}. \tag{16}$$
According to the right panel of Fig. 1 the minimum of the potential along the x-axis ($y = 0$) is located in the middle of the gap, $x_{\min} = r(E) + W(E)/2$ or $x_{\min} = r_o + w/2$. The energy threshold is then given by
$$E_* = V(r_o + w/2) = V_1(r_o + w/2) + V_2(r_o + w/2) = 2/(1 + \exp(w/(2\sigma))).$$
Correspondingly, the maximum velocity is
$$v_{\max}(E) = \sqrt{2(E - V(r_o + w/2))}. \tag{17}$$
This is a function of the energy and independent of the gap size.
2. Alternatively we can define an average velocity according to an average potential in the gap. Due to symmetry, we can calculate the integral of the potential $V_1(x) + V_2(x)$, again along the x-axis, in the first half of the region and average over $W(E)/2$,
$$V_{\text{ave}}(W(E)) = \frac{2}{W(E)} \int_{r(E)}^{r_o + w/2} (V_1(x) + V_2(x))dx.$$
Plugging in the functional forms for V_1 and V_2 we obtain
$$V_{\text{ave}}(E, W(E)) = 2 + \frac{2\sigma}{W(E)} \ln \left[\frac{1 + \exp(r(E) - r_0)/\sigma)}{1 + \exp((L - r(E) - r_o)/\sigma)} \right]. \tag{18}$$
This yields an expression for the velocity that is a function of the energy and the average potential V_{ave} at the exit of the trap,
$$v_{\text{ave}}(E, W(E)) = \sqrt{2(E - V_{\text{ave}}(W(E))}. \tag{19}$$
3. Finally, let us approximate the average velocity in a gap of size $W(E)$ by
$$v = \frac{2}{W(E)} \int_{r(E)}^{r(E)+W(E)/2} \sqrt{2(E - V(r))}dr, \tag{20}$$
where $V(r) = V_1(r) + V_2(r)$. This integral is not solvable analytically, but we can compute it numerically.

Next, we compare our random walk approximations $D_{\text{MZ}}(E)$ and $D_{\text{B}}(E)$ with our numerical results by using these three estimates for the velocities .

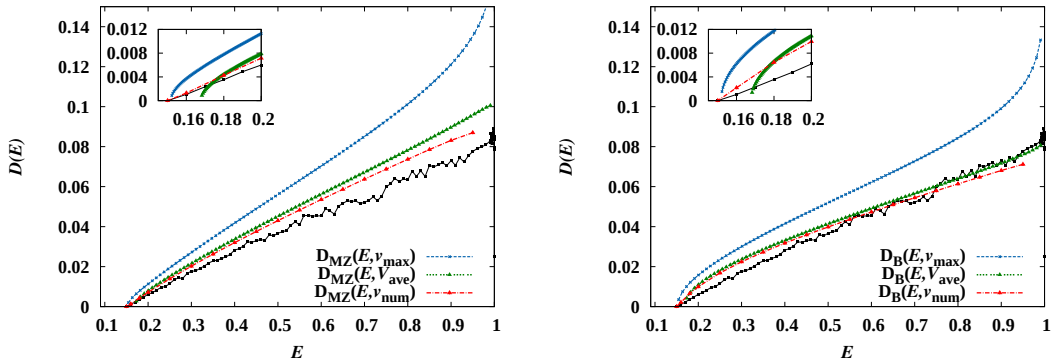

Fig. 3. Diffusion coefficient $D(E)$ as a function of the energy E in the small energy regime $E < 1$. The black (non-smooth) line shows the simulation results obtained from the same input parameters as in Fig 2. Left panel: Machta-Zwanzig random walk approximation $D_{\mathrm{MZ}}(E)$ given by Eq. (12). Right panel: Boltzmann random walk approximation $D_{\mathrm{B}}(E)$ given by Eq. (15). For each case three different approximations of the velocities have been used as described in the text.

3.3 Comparison between random walk approximations and numerical results

The approximations based on D_{MZ} with different velocities are compared to simulation results for the diffusion coefficient with $E \leq 1$ in the left panel of Fig. 3. As expected, D_{MZ} with an average velocity does not reproduce the onset of diffusion where $D = 0$ while D_{MZ} that uses a maximum velocity recovers the threshold (see the inset). The approximation D_{MZ} with the maximum velocity is not accurate indicating that not many particles travel with the maximum velocity but with some average velocity instead. According to the inset, $D_{\mathrm{MZ}}(E, v_{\mathrm{num}})$ captures the threshold and especially gives the correct asymptotics when $E \to E_*$.

The approximations of D_{B} with three different velocities are shown in the right panel of Fig. 3. The result obtained by using the average velocity agrees well with the numerical data at larger energies $E \to 1$. Note that in this system we use a smoothness of $\sigma = 0.01$, which produces a smooth steep potential similar in structure to the hard Lorentz gas, at least for energies smaller than the maximum of the potential. Therefore particles are more likely to travel by "free flights" before getting close to a scatterer. This explains why D_{B} is a better approximation than D_{MZ}. However, our Boltzmann approximation fails to reproduce $D(E)$ as the energy approaches the onset of diffusion, since the approximation is based on collisionless flights, and τ_c is defined even when $E < E_*$. D_{B} still manages to capture the threshold with $v_{\max}$ and v_{ave}, but the shapes of the curves do not match (see the inset). We remark that the impact of varying the smoothness on diffusion in the soft Lorentz gas has been investigated in Refs. [48,52].

4 Diffusion coefficient for intermediate energies

Next we explore the regime of intermediate energies, i.e., $1 < E < 2$. According to Fig. 2 the diffusion constant has a clear kink with changing curvature at $E = 1$ suggesting a mechanism of diffusion that is different from the small energy regime as the energy passes this value. A key feature of this regime is that at energies below $E = 1$ particles cannot pass the maxima of the potential but are restricted to a certain area in configuration space, which we called traps. However, when the total energy starts to exceed $E = 1$ a particle can cross all these maxima, which generates a novel regime of diffusion.

In Fig. 4 we first show numerical results of the MSD as a function of time t around $E = 1$. In all cases the MSD shows normal diffusion in the long time limit, although there are some features that distinguish the regimes of $E < 1$ from $E > 1$. In particular, there is a transient in the MSD at energies $E \geq 1.001$, which is not present at $E \leq 1$. Note that at $E = 1 + \epsilon$,

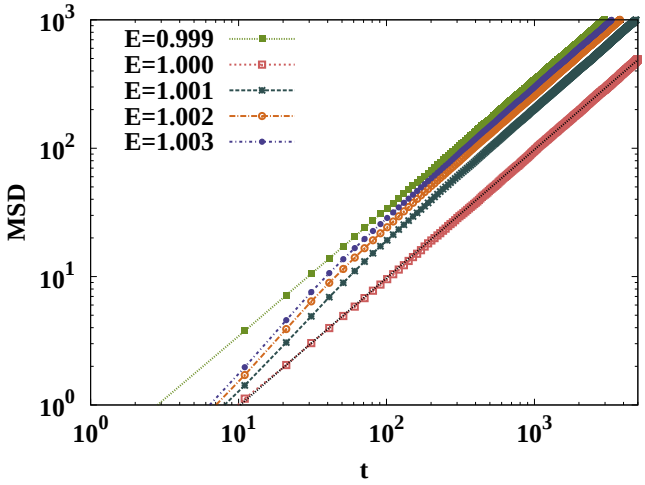

Fig. 4. Numerical results for the mean square displacement (MSD) as a function of time t for different energies E in the transition zone close to $E = 1$. The input parameters are the same as in Fig. 2.

$\epsilon > 0$, the area available in the configuration space becomes unbounded, that is, particles with energies $E > 1$ are allowed to travel everywhere, even in regions very close to the centre of a scatterer. When reaching this position, however, particles have very small but non-zero kinetic energy. This causes an unstable trapping mechanism, which suppresses diffusion when $E \to 1$.

We can now construct a random walk approximation for diffusion in this regime based on traps of slow motion. For this purpose, we need to redefine a trap *on a scatterer* and also to compute the average rate at which a particle leaves this trap. It is not straightforward to exactly determine the area where this trapping occurs, since this depends on how one defines "slow motion". The potential is radially symmetric at each lattice point, hence let us assume that the trapping mechanism takes place on a circle with some radius r_s centered at each scatterer. According to the definition of our Fermi-type scatterer, $\sigma \to 0$ corresponds to enlarging the top of the potential. Let us take a constant value $r_s = 1 = r_o$ as our first approximation for the radius of the circle.

We first need to calculate the velocity of a particle in this region. In order to do so, we assume that inside the circle, or trap, the velocity is constant. The potential energy is (close to) maximal in this circle, therefore the kinetic energy as well as the velocity are (close to) minimal. Hence, $v_{\min} = \sqrt{2(E - V_{\max})}$. The total phase space of the trap is $\Omega = A_\bullet 2\pi v$, where $A_\bullet(r_s)$ is the area of the circle with radius r_s, and v is some constant minimal velocity. Then the available phase space where particles leave the trap in time Δt is

$$\omega = C2v^2,$$

where v is the constant velocity defined above and C is the length of the available portion of the trap where particles escape, i.e., the length of the circumference with radius r_s. Using Eq. (8) we obtain the escape time as

$$\tau(E) = \frac{A_\bullet(r_s)}{2r_s v_{\min}}. \tag{21}$$

We can now substitute Eq. (21) into the random walk approximation for D Eq. (7), where l is considered to be the distance between two traps or centres of scatteres, which in this case is given simply by the geometry of the problem as $l = L = 2r_o + w$. Finally we get

$$D_s(E) = \frac{r_o(2r_o + w)^2}{2A_\bullet(r_s)} v_{\min}(E). \tag{22}$$

In this approximation we see that

$$D_s(E) = \text{const.} \cdot v_{\min}(E) = \text{const.} \sqrt{2(E - V_{\max})}.$$

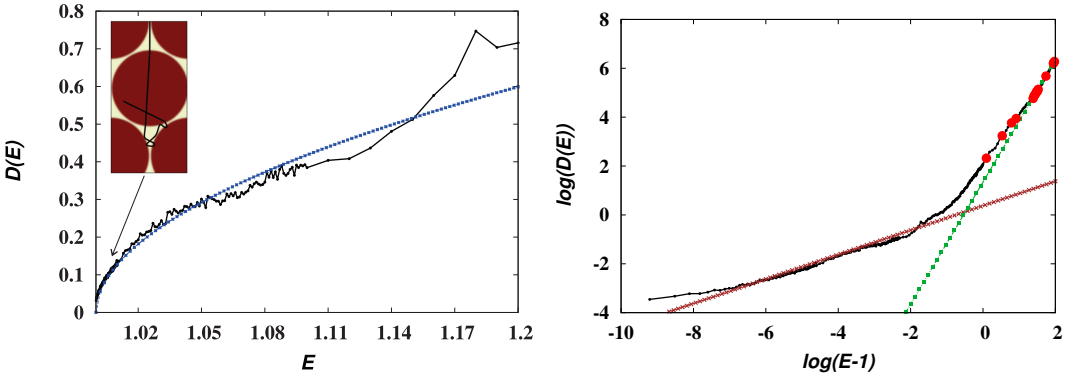

Fig. 5. Diffusion coefficient $D(E)$ in the transition regime $E \to 1^+$ obtained from simulations (black dotted lines) together with our random walk approximation in this regime Eq. (22). Results are given both on linear (left panel) and log-log scales (right panel). In the right panel the red line has a slope 1/2, the green line has slope 5/2, and red circles indicate the presence of islands of stability in phase space. The inset in the left panel shows a typical trajectory in this diffusive regime.

Choosing a constant potential $V = 1$ this expression yields

$$D_{\rm s}(E) \sim \sqrt{E-1}. \tag{23}$$

Let us now compare our numerical results to this approximation when $E \to 1^+$. In the left panel of Fig. 5 we show the numerically obtained diffusion coefficient in the transition regime together with a numerical fit to the data of the form

$$D(E) = a(E-1)^b. \tag{24}$$

With this fit we find an exponent of $b = 0.518$ in the energy interval (1.0001, 1.2). This agrees quite well with the analytical description of Eq. (22). Our approximation makes assumptions on the radius r_s and does not match exactly to the shape of $D(E)$. On the other hand, it reveals the asymptotic form $\sqrt{E-1}$ as $E \to 1^+$. This implies that the motion of particles is dominated by slow motion close to the centres of the scatterers leading to a full suppression of $D(E)$. To see this more clearly, the right panel of Fig. 5 shows $\log D(E)$ as a function of $\log(E-1)$. We observe a regime where the data matches the red line with slope $m = 1/2$, equivalent to the square-root behavior in the linear graph in the left panel. In addition, we find the transition to a different regime where $m = 5/2$ (green line), which we discuss in Sec. 5.

At small values $E \to 1^+$ there is a discrepancy between the simulation data and the randow walk approximation. This is a delicate regime in terms of numerical accuracy. Moreover, our approximation assumes that v is constant in a circle with radius r_s of area $A_\bullet$. While in the approximation there is an abrupt jump at $r_{\rm s}$, the potential that we use for the simulations is a smooth function of the position. Performing numerical simulations with higher precision in this regime and modelling $V_{\rm max}$ as accurately as possible could reduce the difference between the approximation and the data enhanced by the logarithmic scale.

The functional form of $D(E)$ reflects a dynamics where particles travel with small velocity over the top of the scatterers and randomize in the middle of the zones with minimum potential energy, see the inset of Fig. 5. This is supplemented by a contribution from particles that travel in straight lines until they get scattered. The last effect is more pronounced as the energy increases, as we discuss in the following.

5 Diffusion coefficient for high energies

Our final quest is to characterize the diffusion coefficient $D(E)$ for large energies. Here we compare our numerical results to theoretical approximations put forward by Aguer et al. [32]

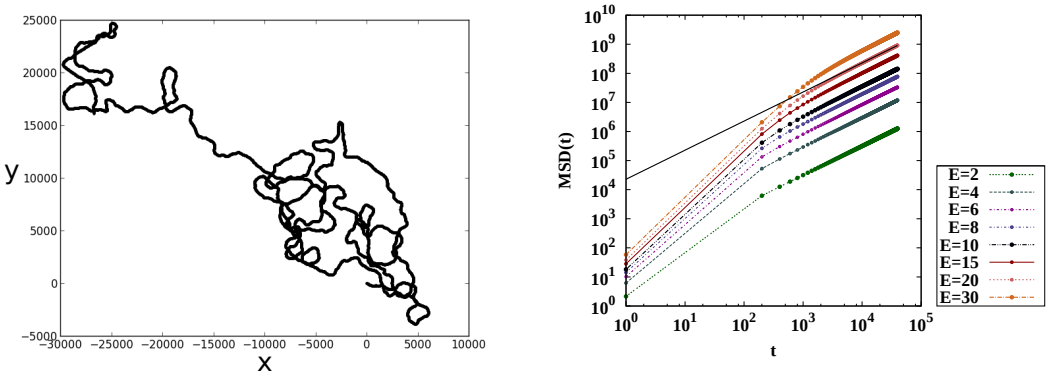

Fig. 6. Left panel: Example of a trajectory at $E = 40$ with iteration time $t = 40000$. Right panel: Time dependence of the mean square displacement (MSD) in the high energy regime. The black line indicates a slope of one.

and Nobbe [31]. For this purpose we need to make sure that we deal with an interval of the energy parameter that exhibits normal diffusion. To illustrate the problem of identifying such energies, we show a typical trajectory at high energies in the left panel of Fig. 6: We see that the particle travels in the same direction for long periods of time by then changing its direction, it repeats this and in the long run generates a random pattern at large scale. This corresponds to the fact that as the energy parameter is increased the particles move faster and consequently travel long distances before changing their direction, meaning the randomization process takes longer than in the small energy regime. But this purely qualitative picture does not guarantee that normal diffusion exists for this or other energy parameters. Quantitatively, the MSD should tell whether there is normal diffusion, which is what we explore next.

In the right panel of Fig. 6 we show the MSD for energies $2 \leq E \leq 30$, which roughly corresponds to the high energy regime of diffusion shown in Fig. 2. The black line indicates a slope equal to one yielding normal diffusion, where according to Eq. (5) the diffusion coefficient $D(E)$ exists. For all these energies the MSD eventually appears to grow linearly in time in the long-time limit yielding $D(E)$ plotted in Fig. 2. However, we see that for higher energies the transition time to the onset of the linear asymptotic regime shifts to considerably longer times: While for $E = 2$ the MSD appears to be linear starting from around $t \sim 10^2$, for $E = 30$ values of t larger than 10^3 are required. It is thus not entirely clear whether there is a linear asymptotic regime for arbitrarily high energies, or whether there exists an energy value starting from which a diffusion coefficient does not exist anymore. Secondly, we can not tell whether the trend of linear growth in time really continues at longer simulation times. That the situation is indeed more subtle becomes clear by looking in detail at the phase space of our model, which gives us a more precise method than simply plotting the MSD to decide about normal diffusion.

Our aim is to check for periodic islands of stability in phase space, which are known to have a major impact on transport properties [11,13,14]. This holds in particular for so-called *accelerator mode islands* [28,12,53], which in our model originate from quasi-ballistic (q-b) trajectories. With a q-b trajectory we mean the path of a particle that travels on average in one direction across the lattice, that is, the path wiggles periodically around a straight line, where the wiggles are due to specific microscopic scattering events; see Fig. 3 in Ref. [48] for explicit examples and Ref. [52] for full details. But even initial conditions outside these stable component that 'stick' to the boundary of an island can have an effect on averages of observables [51,53]. Therefore, if we find islands of stability due to q-b trajectories in configuration space we cannot expect to have normal diffusion in the long time limit [11,13,14,28]. For this reason we need to exclude any parameter values where we find q-b periodic orbits from an analysis of an energy-dependent diffusion coefficient $D(E)$.

In order to find islands of stability in phase space we use the approach via Poincaré surfaces of section (PSoS) as described in Refs. [48,52]. In our case the PSoS is defined by the plane

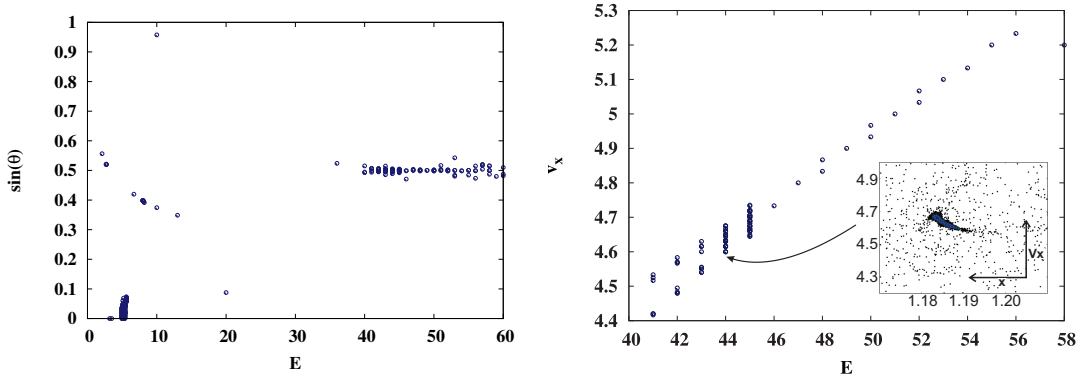

Fig. 7. Islands of stability in phase space: Each circle in both plots represents a potentially stable island in phase space for a given energy parameter E. Left panel: The y-axis indicates the sine of the angle θ between the velocity vector at the moment of exiting the gap and the normal to the boundary. Right panel: As in the left panel but with the velocity component v_x, displaying a backward bifurcation. Inset: Stability island due to a quasi-ballistic trajectory at $E = 44$.

$(x, \sin\theta)$, where x is the position of a particle when it leaves the rhomboid unit cell (see Fig. 1), and as before θ is the angle between its velocity vector and the normal to the boundary. As a constraining numerical factor a given ensemble of initial conditions does not necessarily catch tiny islands of stability: The smaller the island, the more difficult it is to detect it numerically, as it only appears if we choose initial conditions that are in the island. The islands of stability that we find are indeed very tiny, and they correspond to two different types of periodic motion: There are islands related to q-b trajectories, as discussed above, but also other islands that display localized motion. While the latter do not yield anomalous diffusion, the q-b trajectories do [11, 13, 14, 28, 12, 53]. Islands of stability exist for many energy values in our model, in particular, trivial islands generated by the main symmetry channels due to the focusing of the potential walls, and other islands where particles fly over the top of the scatterers.

Our results are summarised in Fig. 7, which shows parameter values where we detect periodic islands of stability. The shapes of their corresponding trajectories vary depending on the energy. The right panel of Fig. 7 depicts a region of the PSoS at $E = 44$ where a stability island is found. The coordinate space trajectories corresponding to this island are almost straight lines, as can be expected due to the high total energy, hence they are not shown. As accordingly the diffusion coefficient $D(E)$ does not exist at these energies, we have plotted red filled circles between respective values of the diffusion coefficient curve in Fig. 2. A more detailed analysis [52] reveals that the structure of the phase space is rich, even for smaller energies.

To find the normal diffusion coefficient $D(E)$ as a function of the energy, Fig. 7 suggests to consider an interval of energies $14 < E < 19$ or $21 < E < 40$. If we ignore the peak at $E = 20$ we can choose $14 < E < 40$. Figure 8 shows numerical results on a double-logarithmic scale together with an error estimate; for details of this estimate see Ref. [52]. The error bars are relatively small. The green line indicates a slope of $m = 5/2$ as predicted in Ref. [32]. Fitting a function of the form aE^m to the numerical data in the intervals of energy $(21, 35)$ yields $m = 2.54$. More fits and their resulting exponents in different energy regimes, together with error estimates, are presented in Table 1.

In Ref. [32] it was concluded that at sufficiently large energies $D(E) \propto E^{5/2}$ while Ref. [31] which, however, applies to attractive potentials, yields $D(E) \propto E^{3/2}$. Overall, the behaviour detected here seems to be very close to the one predicted by the former theory but very different from the latter. By observations of trajectories in configuration space (see the right panel of Fig. 6), our model behaves similarly to the dynamics underlying the model in Ref. [32], where particles travel for long times before changing the direction by a small angle. In contrast, for the model in Ref. [31] particles travel over short distances and change the direction of the path by a large angle. This difference was also noted in Ref. [32]. We note that the simulations in

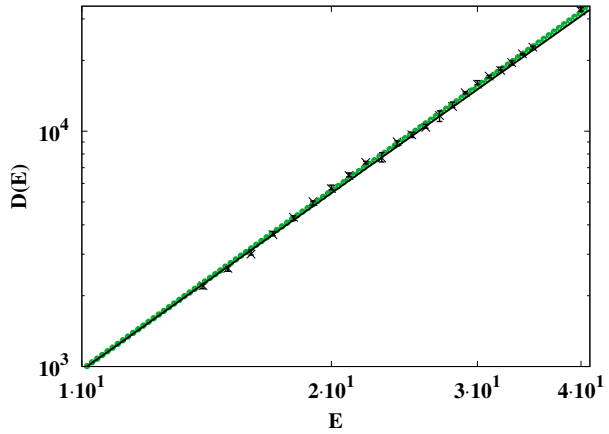

Fig. 8. Diffusion coefficient $D(E)$ obtained from simulations as a function of the energy E. The numerical data is the same as in Fig. 2. The green line indicates a slope of $m = 5/2$ as predicted in Ref. [32].

Table 1. Exponent m in $D(E) = aE^m$ obtained from fits to the simulation data over different intervals of energies E. The last column indicates the error of the fits.

Energy	m	$+/-$
$2 < E < 35$	2.524	0.0188
$14 < E < 40$	2.540	0.0186
$21 < E < 35$	2.521	0.0376
$21 < E < 40$	2.545	0.0257

the latter work always yielded normal diffusion even for large energies. This is due to the model used therein, where there is no mechanism of generating islands in phase space.

6 Conclusions

We have studied diffusion in a soft periodic Lorentz gas in which the hard walls of the conventional Lorentz gas scatterers were replaced by repulsive Fermi potentials. Our goal was to understand how diffusion depends on varying the energy as a control parameter in this system. For this purpose we computed the diffusion coefficient as a function of the total energy of a particle from simulations. We compared our numerical results with simple analytical random walk approximations.

We distinguished three different diffusive regimes: (1) For small energies, i.e., when the energy is less than the maximum of the Fermi potential, there is an onset of diffusion which is well approximated by a random walk approximation put forward by Machta and Zwanzig [49] based on a simple phase space argument. For slightly larger energies the energy dependence of the diffusion coefficient is well explained by a Boltzmann-type random walk approximation which employs a collisionless flight argument. (2) There is a specific value of the energy at which a particle can for the first time travel over the top of a Fermi potential. This defines the onset of a second diffusive regime, where a particle is getting trapped on the top of each potential. In this regime we observe a full suppression of diffusion with a square root dependence on the energy, as is explained by another simple random walk argument similar to the one of Machta and Zwanzig. (3) For large energies the energy-dependent diffusion coefficient yields a power law $D(E) \propto E^{5/2}$ in agreement with the random walk argument presented in Ref. [32]. On top

of this dynamics there are parameter regions exhibiting superdiffusion which, however, were not the focus of our present study.

We remark that we have also studied energy-dependent diffusion in this soft Lorentz gas with a second, different setting of parameters modeling a shallower potential. Here we observed that for small energies the Boltzmann approximation is in general a better approximation outperforming the one by Machta and Zwanzig for all energies even at the onset of diffusion [52]. However, for these parameters q-b islands start to appear even at smaller energies. Our numerical results furthermore suggest that islands of stability in phase space are ubiquitous for large enough energies, irrespective of particular values of the other parameters. We also observed that at large enough energies the size of the islands increases with the energy, in agreement with Ref. [37]. This will profoundly obscure the underlying dependence of the diffusion coefficient as a function of the energy in this regime.

An interesting open question is to determine the precise type of superdiffusion for parameter regions with islands in phase space by matching the simulation data to predictions of a stochastic model, such as Lévy walks [54]. Secondly, it would be exciting if these different diffusive regimes could be detected in experiments, e.g., of diffusion in molecular graphene. Here perhaps the temperature of the system could be varied mimicking our variation of the total energy of a particle. Especially the suppression of diffusion at intermediate energies should be a phenomenon that would be interesting to be observed in experiments.

S.G.G. acknowledges support from the Mexican National Council for Science and Technology (CONACyT) by scholarship no. 262481. R.K. thanks Prof. Krug from the U. of Cologne and Profs. Klapp and Stark from the TU Berlin for hospitality as a guest scientist as well as the Office of Naval Research Global for financial support. He also acknowledges funding from the London Mathematical Laboratory, where he is an External Fellow.

The first and the second author designed the research. All authors performed the research, but the first author contributed the majority to it. The computer code (published separately) was provided by the team around the last author. All authors analysed the data, The first author wrote the manuscript, supported by all others.

References

1. J.R. Dorfman, *An introduction to chaos in nonequilibrium statistical mechanics* (Cambridge University Press, Cambridge, 1999)
2. P. Gaspard, *Chaos, scattering, and statistical mechanics* (Cambridge University Press, Cambridge, 1998)
3. R. Klages, *Microscopic chaos, fractals and transport in nonequilibrium statistical mechanics* (World Scientific, Singapore, 2007)
4. R. Klages, J.R.Dorfman, Phys. Rev. Lett. **74**, 387-390 (1995)
5. R. Klages and J.R. Dorfman, Phys. Rev. E **59**, 5361-5383 (1999)
6. J. Groeneveld and R. Klages, J. Stat. Phys. **109**, 821-861 (2002)
7. B. V. Chirikov, Phys. Rep. **52**, 263-379 (1979)
8. A.B. Rechester, M.N. Rosenbluth and R.B. White, Phys. Rev. A **23**, 2664-2672 (1981)
9. J.A. Blackburn, N. Grønbech-Jensen, Phys. Rev. E *53*, 3068-3072 (1996)
10. F. Cagnetta, G. Gonnella, A. Mossa, S. Ruffo, Europhys. Lett. **111**, 10002 (2015)
11. A. Zacherl, T. Geisel, J. Nierwetberg, and G. Radons, Phys. Lett. **114A**, 317-321 (1986)
12. T. Manos and M. Robnik, Phys. Rev. E **89**, 022905 (2014)
13. G. Zaslavsky, Phys. Rep. **371** 461 (2002).
14. R. Klages, G. Radons, and I.M. Sokolov (editors), *Anomalous transport: Foundations and Applications* (Wiley-VCH, Berlin, 2008)
15. D. Szasz (editor), *Hard-ball systems and the Lorentz gas* (Springer, Berlin, 2000)
16. H.A. Lorentz, Acad. Amst., **7**, 438-453 (1905)
17. L.A. Bunimovich, Ya. Sinai, Commun. Math. Phys. **78**, 247-280 (1980)
18. P. Gaspard, G. Nicolis, Phys. Rev. Lett. **65**, 1693-1696 (1990)
19. R. Klages and C. Dellago, J. Stat. Phys. **101**, 145-159 (2000)

20. T. Harayama, R. Klages, P. Gaspard, Phys. Rev. E **66**, 026211 (2002)
21. R. Klages and N. Korabel, J. Phys. A: Math. Gen. **35**, 4823–4836 (2002)
22. C. Dettmann, Commun. Theor. Phys. **62**, 521 (2014)
23. T. Harayama and P. Gaspard, Phys. Rev. E, **64**, 036215 (2001)
24. L. Mátyás and R. Klages, Physica D **187**, 165 (2004)
25. P. Gaspard and R. Klages, Chaos, **8**, 409-423 (1998)
26. D. Turaev and V. Rom-Kedar, Nonlin. **11**, 575 (1998)
27. V. Rom-Kedar, D. Turaev, Physica D **130**, 187 (1999)
28. A.J. Lichtenberg and M.A. Lieberman, *Regular and chaotic dynamics*, 2nd Edition (Springer, New York, 1992)
29. A. Kaplan, N. Friedman, M. Andersen, N. Davidson, Physica D **187**, 136145 (2004)
30. A. Knauf, Commun. Math. Phys. **110**, 89-112 (1987)
31. B. Nobbe, J. Stat. Phys. **78**, 1591-1605 (1995)
32. B. Aguer, S. De Bievre, J. Phys. A: Math. Theor. **43(47)**, 474001 (2010)
33. B. Bagchi, R. Zwanzig, M. C. Marchetti, Phys. Rev. A, **31**, 892-896 (1985)
34. T. Geisel, A. Zacherl, G. Radons. Phys. Rev. Lett., **59**, 2503-2507 (1987)
35. T. Geisel, A. Zacherl, G. Radons, Z. Phys. B, **71**, 117-127 (1988)
36. T. Geisel, J. Wagenhuber, P. Niebauer, G. Obermair, Phys. Rev. Lett. **64**, 1581-1584 (1990)
37. N. C. Panoiu, Chaos **10**, 166-179 (2000)
38. J. Yang, H. Zhao, J. Stat. Mech.: Theor. Exp. **12**, L12001 (2010)
39. P.R. Baldwin, Physica D **29**, 321 (1988)
40. A. Lorke, J.P. Kotthaus, and K. Ploog, Phys. Rev. B **44**, 3447-3450 (1991)
41. D. Weiss, M.L. Roukes, A. Menschig, P. Grambow, K. von Klitzing, G. Weimann, Phys. Rev. Lett. **66**, 2790–2793 (1991)
42. R. Fleischmann, T. Geisel, R. Ketzmerick, Phys. Rev. Lett. **68**, 1367–1370 (1992)
43. M. Fließer, G.J.O. Schmidt. H. Spohn, Phys. Rev. E **53**, 5690–5697 (1996)
44. M. Gibertini, A. Singha, V. Pellegrini, M. Polini, G. Vignale, A. Pinczuk, L. N. Pfeiffer, K. W. West, Phys. Rev. B **79**, 241406 (2009).
45. E. Räsänen, C. A. Rozzi, S. Pittalis, G. Vignale, Phys. Rev. Lett. **108**, 246803 (2012).
46. K. K. Gomes, W. Mar, W. Ko, F. Guinea, H. C. Manoharan, Nature **483**, 306 (2012).
47. S. Paavilainen, M. Ropo, J. Nieminen, J. Akola, E. Räsänen, Nano Letters. **16**, 3519-3523 (2016)
48. R. Klages, S. Gil-Gallegos, J. Solanpää, M. Sarvilahti, E. Räsänen, submitted for publication (2018).
49. J. Machta and R. Zwanzig, Rev. Lett. **50**, 1959-1962 (1983)
50. J. Solanpää, P. Luukko, E. Räsänen, Phys. Commun. **199**, 133-138 (2016)
51. V. Rom-Kedar, G. Zaslavsky, Chaos **9** 697-705, (1999)
52. S. Gil-Gallegos, Doctoral dissertation, Queen Mary University of London (2018)
53. M. Harsoula, G. Contopoulos, Phys. Rev. E **97**, 022215 (2018)
54. G. Cristadoro, T. Gilbert, M. Lenci, and D. P. Sanders, Europhys. Lett. **108**, 50002 (2014)